

# An AC Input Switching-Converter-Free LED Driver With Low-Frequency-Flicker Reduction

Yuan Gao, *Student Member, IEEE*, Lisong Li, *Student Member, IEEE*, and Philip K. T. Mok, *Fellow, IEEE*

**Abstract**—This paper presents a novel switching-converter-free ac–dc light-emitting diode (LED) driver with low-frequency-flicker reduction for general lighting applications. The proposed driving solution can minimize the system size as it enables the monolithic integration of the controller and power transistors while both the bulky off-chip electrolytic capacitors and magnetics are eliminated. Moreover, the driver can effectively reduce the harmful optical flicker at the double-line-frequency by employing a novel quasi-constant power control scheme while maintaining high efficiency and a good power factor (PF). The proposed driver is implemented with a single controller integrated circuit chip, which includes the controller and high-voltage power transistors, and the off-chip diode bridge and valley-fill circuit. The chip is fabricated with a  $0.35\text{-}\mu\text{m}$  120-V high-voltage CMOS process and occupies  $1.85\text{ mm}^2$ . The driver can provide up to 7.8-W power to the LED and achieves 87.6% peak efficiency and an over 0.925 PF with only 17.3% flicker from a 110-V<sub>ac</sub> 60-Hz input.

**Index Terms**—AC–DC, converter-free, elimination of electrolytic capacitors, flicker reduction, inductor-less, light-emitting diode (LED) driver.

## I. INTRODUCTION

THE light-emitting diode (LED), as the new generation of light source with a rapid growing market, has demonstrated its superiority over its conventional counterparts in terms of energy efficiency, life-time, and eco-friendliness. In many LED systems for general lighting applications, the power is provided from ac mains electricity. Therefore, an ac–dc LED driver is always needed as a power transfer interface between the grid and the LED chips.

A high-performance LED driver should be able to deliver and regulate the power to the LED with high efficiency. Meanwhile, it should also be able to derive as much real power as possible from the ac grid to reduce energy loss, in other words, have a good power factor (PF) [1]. In addition, for the ac powered lighting systems, another crucial design concern is the optical flicker at the line frequency or its harmonics. While the line frequency flicker can be easily eliminated with the help of the full bridge rectification, it is also of importance for the driver to minimize the flicker at the double-line-frequency

Manuscript received July 18, 2016; revised November 22, 2016; accepted January 11, 2017. Date of publication February 13, 2017; date of current version April 20, 2017. This paper was approved by Associate Editor Anthony Chan Carusone. This work was supported by a grant from the Research Grants Council of the Hong Kong Special Administrative Region, China, under Theme-Based Research Scheme through Project T23-612/12-R.

The authors are with the Department of Electronic and Computer Engineering, The Hong Kong University of Science and Technology, Hong Kong (e-mail: ygaoad@connect.ust.hk; eelisong.li@ust.hk; eemok@ust.hk).

Color versions of one or more of the figures in this paper are available online at <http://ieeexplore.ieee.org>.

Digital Object Identifier 10.1109/JSSC.2017.2656147

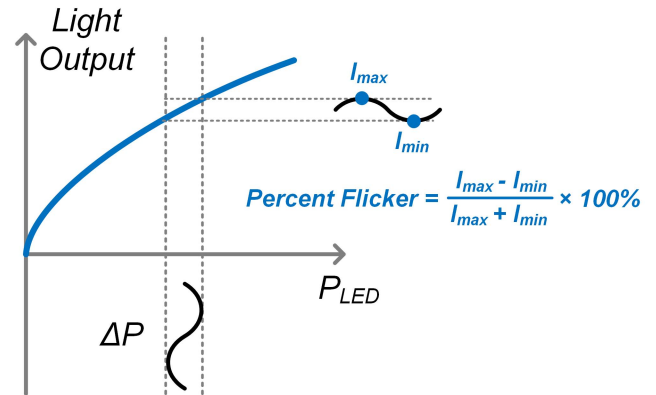


Fig. 1. Relationship between LED electrical power and LED output light intensity, and the definition of percent flicker.

(100 or 120 Hz). Many studies support the claim that the flicker in this frequency range has negative impacts on human health, though it is usually invisible to the naked eye [2]. As shown in Fig. 1, a commonly used measure to evaluate the performance of optical variation in a periodical light output is percent flicker, which is defined as

$$\text{Percent Flicker} = \frac{I_{max} - I_{min}}{I_{max} + I_{min}} \times 100\% \quad (1)$$

where  $I_{max}$  and  $I_{min}$  are the peak and valley values of the light output intensity, respectively. As the LED output light intensity is almost proportional to its electrical power, a small optical flicker can be achieved in the driver by stabilizing the power delivered to the LED [3].

Besides the above-mentioned considerations, system miniaturization has always been a crucial design target for LED drivers, especially for those in low to moderate power lighting systems, which are more sensitive to volume and cost. For ac mains powered LED drivers, the key to achieving miniaturization is to integrate, reduce, or even rule out bulky off-chip components on the printed circuit board (PCB), including power magnetics, aluminum electrolytic capacitors, and power transistors [4]. Moreover, the elimination of those components, especially electrolytic capacitors, will also significantly improve the system reliability [5]. Plenty of ac–dc LED drivers with a variety of topologies or advanced devices to realize high-level system integration have been previously reported [6]–[12]. However, other performance measures, such as PF, efficiency, and flicker in most cases, have to be compromised in these designs.

In this paper, a novel switching-converter-free LED driver without off-chip transistors, magnetics, and electrolytic

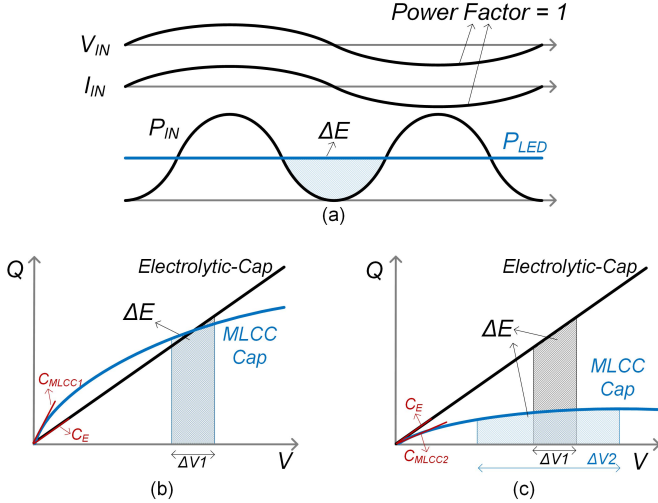


Fig. 2. General considerations for eliminating electrolytic capacitor in the ac powered LED drivers. (a) Key waveforms of ideal driver. (b) Replacing electrolytic capacitor with MLCC capacitor in the same driving topology. (c) Replacing electrolytic capacitor with MLCC capacitor in the capacitance-efficient driving topology.

capacitors, thereby achieving significant volume saving, is demonstrated. At the same time, it is able to offer high efficiency, a good PF and small optical flicker.

This paper is organized as follows. The prior ac-powered LED drivers are reviewed in Section II. The proposed switching-converter-free LED driving architecture is introduced and illustrated in Section III, and the detailed circuit implementation of the system is described in Section IV. Experimental results are shown in Section V. Finally, the conclusion is made in Section VI.

## II. REVIEW OF PRIOR SOLUTIONS

In this section, the general considerations for getting rid of the bulky and unreliable electrolytic capacitors in ac-powered LED drivers will be discussed first. Then, both conventional inductive switching-converter-based solutions and the converter-free approach will be reviewed in detail.

### A. Design Considerations for Replacing the Electrolytic Capacitors

An ideal driver is taken as an example to better understand the challenge to remove the electrolytic capacitors in the system. As shown in Fig. 2(a), this ideal driver forces its input current  $I_{IN}$ , completely matching the ac voltage  $V_{IN}$  to get a perfect unity PF. Meanwhile, the driver offers a stable output power to the LED to minimize the optical flicker. As a result, an energy difference  $\Delta E$  always exists in every half line cycle. To fill this energy difference, the driver has to include some passive components as the power buffer. Usually, capacitor rather than magnetics is preferred because of its effectiveness in terms of lowering volume and cost. Considering the requirements of a high voltage rating and high capacitance, electrolytic capacitors are widely employed in many conventional drivers to filter the energy ripple. However, the poor lifetime of electrolytic capacitors also leads to failure

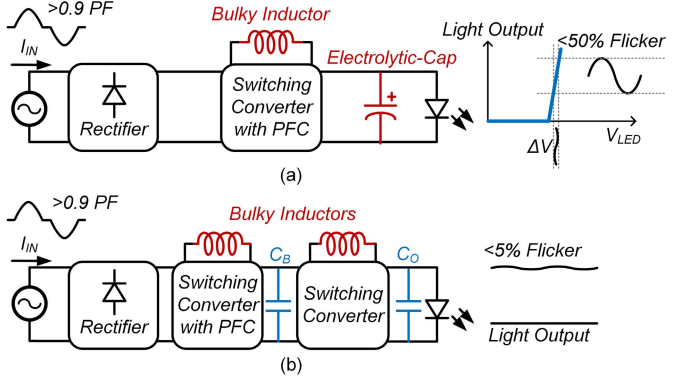


Fig. 3. System diagram of the conventional switching-converter-based LED driving solutions. (a) Single-stage. (b) Two-stage.

of these drivers in a much shorter time than the LED and the driver chip's life expectancy.

Multiple-layer ceramic capacitor (MLCC) is a good alternative to electrolytic capacitor for both system miniaturization and lifetime considerations, but as shown in Fig. 2(b), it suffers from capacitance reduction ( $C = \Delta Q/\Delta V$ ) as the operation voltage goes up, where  $Q$  and  $V$  are the charge and voltage across the capacitor. This means that several times larger rating capacitance, and a higher cost, are required for replacing an electrolytic capacitor with an MLCC capacitor in the same topology. Therefore, to replace electrolytic capacitor with affordable MLCC capacitors, we need to find a driving scheme that can effectively utilize the buffer capacitors [3], [6]. As shown in Fig. 2(c), if the driver can allow a larger voltage ripple (from  $\Delta V1$  to  $\Delta V2$ ) on the buffer capacitor, the requirement of capacitance value will be greatly alleviated (from  $C_{MLCC1}$  to  $C_{MLCC2}$ ).

### B. Switching-Converter-Based LED Drivers

Fig. 3 shows typical single-stage and two-stage switching converter-based LED drivers. In the single-stage solution shown in Fig. 3(a), the converter mainly uses the PF correction (PFC) to regulate the input current in phase with the input line wave, thereby achieving high PF. However, this converter with PFC will deliver nonuniform power to its output and all the energy difference  $\Delta E$  has to be filtered by the capacitor located in parallel with the LEDs. What is worse, as shown in Fig. 3(a), a small voltage ripple on the LEDs will result in significant output light variation. Thus, most of the lighting devices with this type of driver have flicker ranging from 20% to 50% even with the help of several hundreds of microfarads electrolytic capacitors for several watts application. It is inefficient and unaffordable to use MLCC capacitors in this single-stage solution.

The two-stage solution is shown in Fig. 3(b). Besides the PFC stage, another stage is placed to regulate the LED power to reduce flicker. Since the buffer capacitor  $C_B$  is separated from the LEDs and large ripple is allowed on it, it is possible to use MLCC capacitors instead of electrolytic capacitors in this solution. However, not only is the efficiency significantly degraded, but there is also a volume and cost penalty for this extra stage.

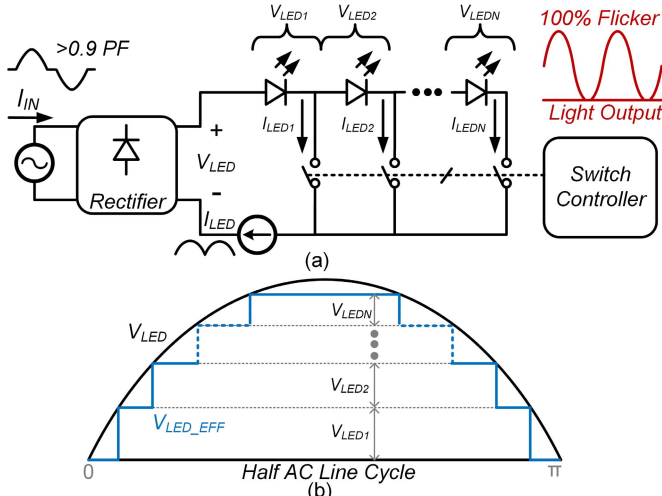


Fig. 4. (a) System diagram and (b) key waveforms of conventional converter-free LED driving solution.

Miniaturization of magnetics is another challenge for designing a switching-converter-based driver. Pushing the switching frequency to several megahertz or even tens of megahertz is a straightforward approach to reduce the inductance, but it will incur a significant increase in switching loss on the power switches and ac loss on the magnetics. In addition, the volume of the magnetics may not scale down monotonically with the inductance as the requirement for the operation frequency is also increased. To solve the switching loss issue, many research efforts have been made with soft switching techniques and/or with advanced devices, such as gallium nitride switches [6]–[8]. However, the magnetics and off-chip power switches still occupy most of the volume of the driving circuit in these designs.

### C. Switching-Converter-Free LED Drivers

Another type of LED driver, called a switching-converter-free LED driver, eliminates the usage of inductive switching converters in the system [10]–[12]. In contrast to the converter-based drivers, the converter-free driver can remove both the power magnetics and electrolytic capacitors from the system. As shown in Fig. 4(a), it usually consists of a string of LEDs in series, several switches, a switch controller, and a rectified sine-wave current source. The controller can bypass part of the LEDs by opening or closing the switches according to the input voltage, so at any time of each cycle, most of the power from ac mains will be delivered to the LEDs rather than be consumed by switches or the current source. However, because no power buffer is used in the driver, it inherently has 100% flicker at the double-line-frequency, as shown in the figure.

## III. PROPOSED LED DRIVING SYSTEM

In view of the drawbacks of conventional ac-powered LED drivers, it is needed to develop a new driver for achieving a high level integration of LED driver without degrading the performance of PF, flicker, or efficiency. Fig. 5 shows

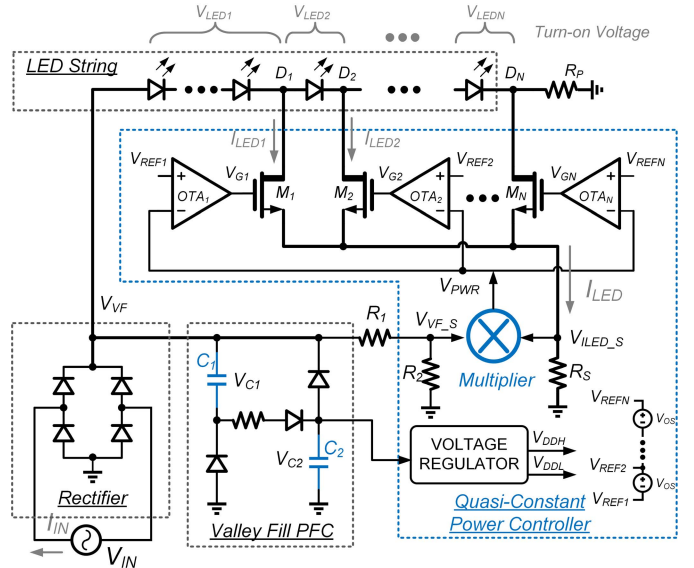


Fig. 5. System diagram of the proposed switching-converter-free LED driver.

the system diagram of the proposed switching-converter-free LED driver [13]. The key part of the proposed design is the quasi-constant power (QCP) controller, which is capable of regulating the total power on the LED while solving the flicker issue of conventional converter-free drivers.

The operation principle of the proposed driver can be explained with the help of the waveform diagram in Fig. 6. As shown in Fig. 5, a diode bridge is used for ac voltage rectification and a passive valley-fill power correction circuit (VFC) is placed after the bridge to achieve a good PF. Meanwhile, the capacitors  $C_1$  and  $C_2$  in the VFC serve as the power buffer to provide enough voltage to power the LED string. As shown in Fig. 6, the VFC charges  $C_1$  and  $C_2$  in series when the input line is high in every cycle, and discharges them in parallel to power the LEDs as the ac line falls below  $V_{C1}$  ( $V_{C2}$ ). Besides the charge and discharge phases,  $C_1$  and  $C_2$  are in a floating state when the input voltage is larger than  $V_{C1}$  ( $V_{C2}$ ) and smaller than the sum of  $V_{C1}$  and  $V_{C2}$ . In this period, the power from the ac line will be directly transferred to the LEDs instead of going through the VFC. As the capacitors in the VFC are separated from the LEDs, it is able to have a larger voltage ripple and thus only requires a smaller capacitance. As discussed in Section II, the compact MLCC capacitors rather than electrolytic capacitors can be used for several watts LED driver as in the case shown in Fig. 2(c).

The LED string is divided into  $N$  high-voltage power MOSFETs  $M_1$  to  $M_N$ . The turn-on voltages of each segment of LED are  $V_{LED1}, V_{LED2}, \dots, V_{LEDN}$ , respectively. The sum of the turn-on voltages of all segments should be close to the peak input voltage. A resistor  $R_P$  is connected to the end of the LED string to provide a current path for protecting the IC from high voltage breakdown during the startup procedure; otherwise, the on-chip nodes from  $D_1$  to  $D_N$  may suffer from intolerable high voltage close to  $V_{VF}$  as all the power MOSFETs are turned OFF.

The QCP controller processes two tasks at the same time. One is to ensure efficient power transfer while the other is

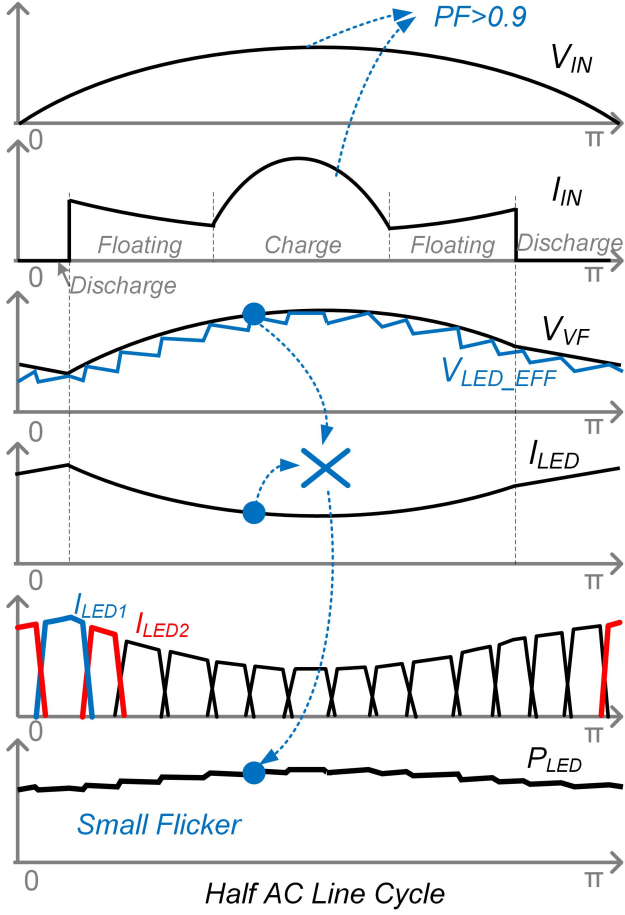


Fig. 6. Diagram of key waveforms for the proposed driver.

to stabilize the output power. The first task is completed by the multiple regulation loops formed by OTAs and power MOSFETs. As  $V_{VF}$  changes, the multiple loops intelligently select the maximum number of LEDs that can light up, so the loss on the MOSFETs can be minimized and the effective voltage across the LED string  $V_{LED\_EFF}$  is almost the same with  $V_{VF}$  as shown in Fig. 6. The second task of the QCP controller is to reduce the variation of the LED light output by regulating the total LED power. The controller senses the voltage on the LED string  $V_{VF}$  and LED current  $I_{LED}$ , and utilizes a multiplier to obtain the LED power, product of the voltage and current,  $V_{PWR}$ . Then,  $V_{PWR}$  is fed back to the multiple regulation loops to push the  $I_{LED}$  in the opposite direction to  $V_{VF}$  to keep the total LED power almost constant. In other words, a higher input voltage will power up more LEDs on the string, but decrease the current on each LED, and vice versa. Thus, a small light output variation is achieved even with significant input voltage ripple.

Fig. 7 gives an example to explain how the QCP controller works in detail. First, assuming that  $V_{VF}$  is capable of turning ON the first segment of LEDs, but not high enough to turn ON the second segment, all the LED current will go through  $M_1$ . As shown in Fig. 7(a), OTA<sub>1</sub>, the multiplier,  $M_1$  and  $R_S$  form a negative feedback loop, and in this case  $V_{PWR}$  will be regulated to  $V_{REF1}$ . Then, when  $V_{VF}$  goes up to a higher voltage, which is high enough to turn ON the second segment,

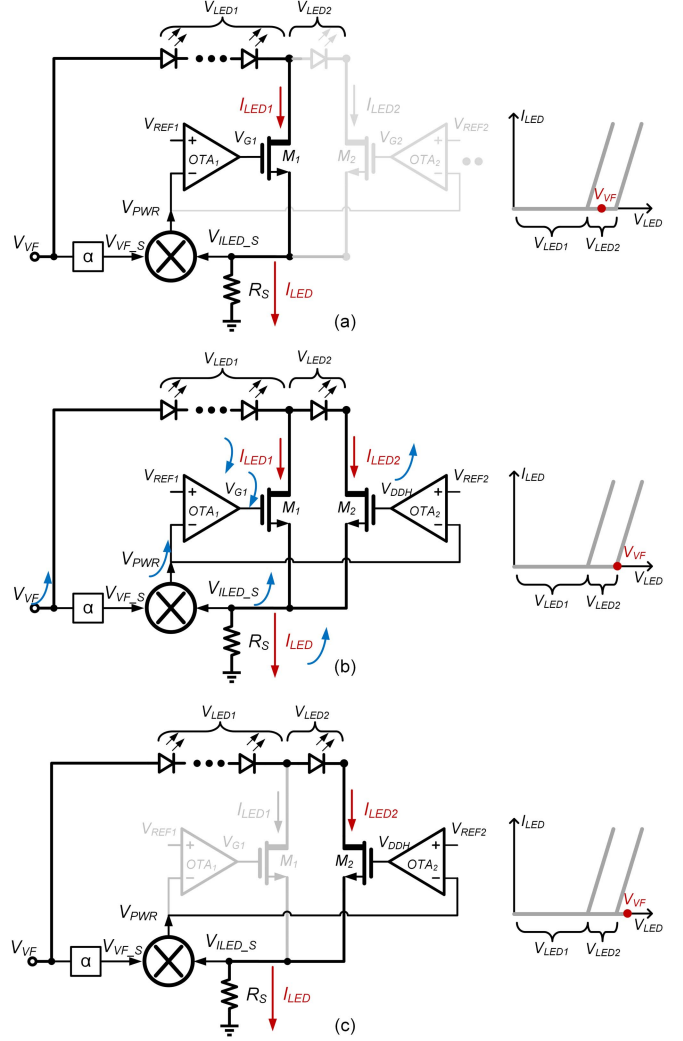


Fig. 7. Example of transition between two branches as input voltage changes.

the LED current will go through both  $M_1$  and  $M_2$ . As  $V_{REF2}$  is designed slightly higher than  $V_{REF1}$ , about 20 mV, the  $M_2$  is fully turned ON by OTA<sub>2</sub>. As shown in Fig. 7(b),  $I_{LED2}$ , as well as  $V_{PWR}$ , goes up very fast with the input voltage, forcing  $I_{LED1}$  to be reduced. Finally, after the amplification of OTA<sub>1</sub> and OTA<sub>2</sub>,  $I_{LED2}$  is much larger than  $I_{LED1}$  and  $M_1$  will be fully turned OFF. As a result, the controller is dominated by the loop formed by  $M_2$  and OTA<sub>2</sub>, as shown in Fig. 7(c). Owing to the high gain of OTA<sub>2</sub>,  $V_{PWR}$  will be regulated to  $V_{REF2}$ . The operation principle is similar when  $V_{VF}$  goes down from high to low. As the reference voltages only have a small variation (e.g.,  $V_{REF1} = 2$  V and  $V_{REF2} = 2.02$  V), the LED power can be regulated as a quasi-constant value in each cycle. Therefore, it is possible to achieve a very small light flicker.

#### IV. CIRCUIT IMPLEMENTATION

##### A. LED Segment Optimization

The proposed switching-converter-free driver shown in Fig. 5 is designed to power a string of LEDs in a series connection. These LEDs are divided into  $N$  segments by the on-chip power transistors  $M_1-M_N$ . A practical strategy is needed to determine the segment number  $N$ , the total number

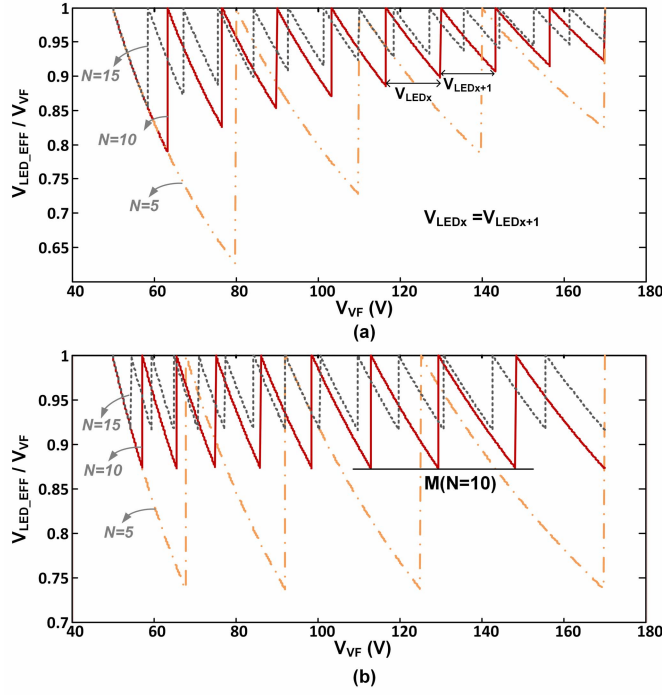


Fig. 8. Simulated plots of  $V_{LED\_EFF}$  to  $V_{VF}$  ratio with (a) equal segment voltage distribution and (b) efficiency optimized segment voltage distribution.

of LED on the string and how to allocate the LEDs to these segments.

First, the sum of the turn ON voltage of all LEDs on the string should be close to the peak input voltage  $(V_{VF})_{PEAK}$  to minimize the wasted energy on the power transistors

$$\sum_{i=1}^N V_{LEDi} \approx (V_{VF})_{PEAK}. \quad (2)$$

Second, the turn ON voltage of the first segment  $V_{LED1}$  is limited by the affordable peak current of the LED and the breakdown voltage of transistor  $M_1$ . Taking this specific implementation as an example, the driver is designed to work at 100–120 V<sub>ac</sub> (peak voltage 170 V) with the 120-V on-chip MOSFET. Then,  $V_{LED1}$  should be larger than 50 V.

After the first segment, the other LEDs can be allocated with different approaches. One straightforward implementation is the equal distribution of these LEDs. However, as shown in Fig. 8(a), this approach will suffer a larger efficiency (ratio of  $V_{LED\_EFF}$  to  $V_{VF}$ ) drop when the input voltage  $V_{VF}$  is low. The valley points in the whole input range can be written as

$$\left( \frac{V_{LED\_EFF}}{V_{VF}} \right)_x = \frac{\sum_{i=1}^{x-1} V_{LEDi}}{\sum_{i=1}^x V_{LEDi}} \quad (3)$$

where  $x$  can be 2, 3, ...,  $N$ . For the equal distribution approach, apparently, the ratio reaches its minimum value as  $V_{VF}$  becomes close to the sum of  $V_{LED1}$  and  $V_{LED2}$ . To optimize the efficiency of the QCP controller, an alternative approach is adopted for guiding the selection of the LEDs for each segment. As shown in Fig. 8(b), this approach keeps all valley points at the same value  $M$ . From (2) and (3),  $M$  and

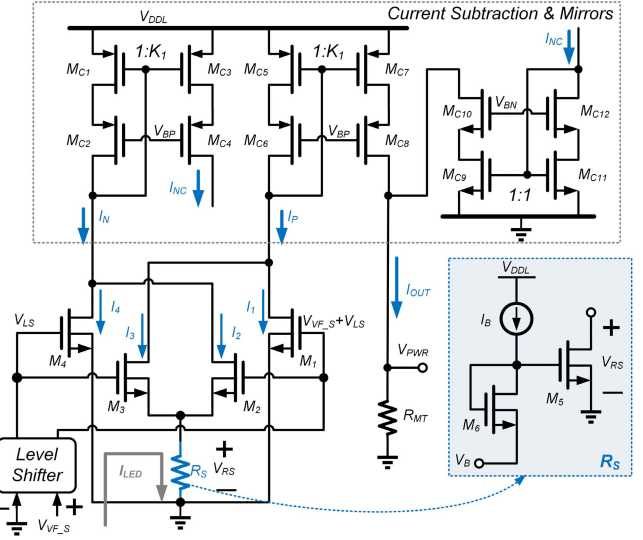


Fig. 9. Circuit diagram of the analog multiplier.

the segment turn ON voltage  $V_{LEDx}$  can be derived as

$$M = \frac{\sum_{i=1}^{x-1} V_{LEDi}}{\sum_{i=1}^x V_{LEDi}} = \frac{\sum_{i=1}^{N-1} V_{LEDi}}{\sum_{i=1}^N V_{LEDi}} = \left( \frac{V_{LED1}}{(V_{VF})_{PEAK}} \right)^{\frac{1}{N-1}} \quad (4)$$

$$V_{LEDx} = V_{LED1} \times \left( \frac{V_{LED1}}{(V_{VF})_{PEAK}} \right)^{\frac{x-1}{N-1}}. \quad (5)$$

For given  $V_{LED1}$  and  $(V_{VF})_{PEAK}$ , it is easy to determine the valley value of the normalized efficiency on Fig. 8(b). The optimal voltage for each segment of LED can also be calculated from (5). In practical implementation,  $V_{LEDx}$  must be a multiple of the single LED voltage, but it is still possible to obtain a near-optimal solution with the above-mentioned equations.

Fig. 8 also shows the comparison of results with different numbers of segments  $N$ . Apparently, the efficiency can be enhanced with more segments. However, it is noted that the improvement gained by adding segments becomes less impressive when  $N$  is already a large number. Meanwhile, more chip area has to be sacrificed for the extra power transistors and I/O pins. In this paper,  $N$  is chosen to be 10, by making a compromise between efficiency and chip size.

### B. Analog Multiplier

Fig. 9 shows the multiplier used in the proposed driver. Four isolated transistors  $M_1$  to  $M_4$  compose the core part of this transconductance multiplier [14], [15]. A level shifter is used for setting a proper dc point for the transistors to ensure that they are working in the saturation region. The drain current of  $M_1$  to  $M_4$  can be written as

$$I_1 = K_N \times (W/L)_1 \times (V_{VF\_S} + V_{LS} - V_{THN})^2 \quad (6)$$

$$I_2 = K_N \times (W/L)_2 \times (V_{VF\_S} + V_{LS} - V_{RS} - V_{THN})^2 \quad (7)$$

$$I_3 = K_N \times (W/L)_3 \times (V_{LS} - V_{RS} - V_{THN})^2 \quad (8)$$

$$I_4 = K_N \times (W/L)_4 \times (V_{LS} - V_{THN})^2 \quad (9)$$

where  $K_N$  is the process transconductance parameter of the n-channel MOSFET. After the current subtraction and

duplication processes shown in Fig. 9, the output voltage of the multiplier  $V_{PWR}$  is given by

$$\begin{aligned} V_{PWR} &= I_{OUT} \times R_{MT} = K_1 \times (I_P - I_N) \times R_{MT} \\ &= K_1 \times (I_1 + I_3 - I_2 - I_4) \times R_{MT} \end{aligned} \quad (10)$$

where  $K_1$  is the copy ratio of the upper current mirror shown in Fig. 9. As shown in Fig. 7, the LED current also goes through the sense resistor  $R_S$ . Compared with  $I_{LED}$ , the current of multiplier  $I_2$  and  $I_3$  can be neglected and thus  $V_{RS} = I_{LED} \times R_S$ . Also, because  $M_1$  to  $M_4$  are fully matched isolated transistors,  $V_{PWR}$  can be rewritten from (6)–(10) as

$$\begin{aligned} V_{PWR} &= 2K_1 \times K_N \times (W/L)_1 \times V_{VF\_S} \\ &\quad \times I_{LED} \times R_S \times R_{MT}. \end{aligned} \quad (11)$$

The multiplication of  $I_{LED}$  and  $V_{VF\_S}$  is achieved with this approach as other parameters in (11) are all independent of the variables  $I_{LED}$  and  $V_{VF}$ . However,  $K_N$  in (11) is a process and temperature-dependent parameter. It means that the LED power will be significantly affected by the process variation and the working conditions. To solve this, an MOSFET-based current sense resistor  $R_S$  is used to compensate for both the process and temperature variation. As shown in Fig. 9, a transistor  $M_5$  with the large size of  $1600/1 \mu\text{m}$  works in the deep-linear mode as a power resistor, and the resistance is given by

$$R_S = \frac{1}{K_N \times (W/L)_5 \times (V_{GS5} - V_{THN})}. \quad (12)$$

A diode-connected transistor,  $M_6$ , is matched with  $M_5$ , but has a smaller size of  $200/1 \mu\text{m}$ . A small current  $I_B$  flows through  $M_6$ , so its gate-source voltage  $V_{GS6}$  is almost equal to the threshold voltage  $V_{THN}$ . The body and source of  $M_6$  is biased to a stable reference voltage  $V_B$  which is designed to 3 V and generated off-chip in this design. Therefore, (12) can be rewritten as

$$\begin{aligned} R_S &= \frac{1}{K_N \times (W/L)_5 \times (V_{GS6} + V_B - V_{THN})} \\ &\approx \frac{1}{K_N \times (W/L)_5 \times V_B}. \end{aligned} \quad (13)$$

The output of multiplier  $V_{PWR}$  can be written as

$$V_{PWR} \approx \frac{2K_1 \times (W/L)_1 \times I_{LED} \times V_{VF\_S} \times R_{MT}}{(W/L)_5 \times V_B}. \quad (14)$$

As an off-chip resistor with low temperature sensitivity was used for  $R_{MT}$ , the gain of this multiplier will only be dominated by the transistor size ratio and reference voltage  $V_B$ .

The simulated waveforms of LED power with the ideal current sense resistor ( $R_S$  is process and temperature independent) and a revised process and temperature compensated resistor are compared in Fig. 10. The results verify that the process and temperature variation of the LED power can be greatly reduced with the help of the compensated resistor.

### C. Operational Transconductance Amplifier

Fig. 11 shows the OTA used in the proposed driver. A revised folded cascode topology with two voltage power

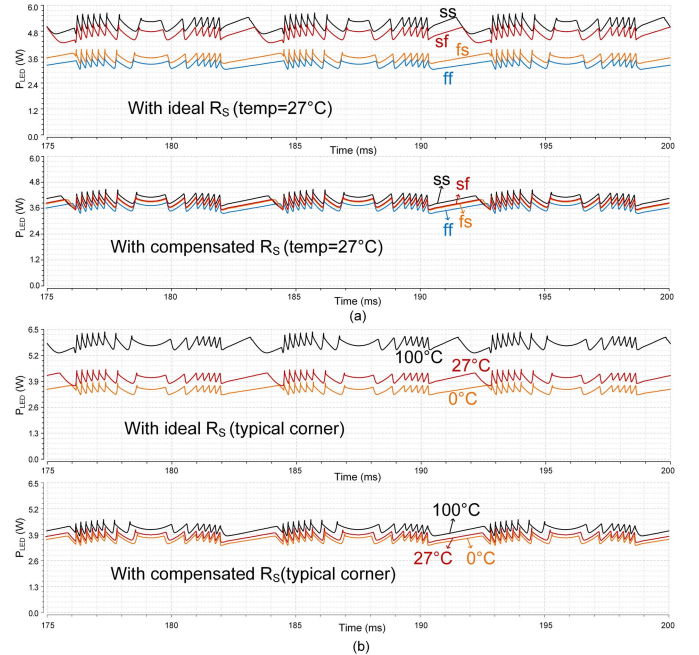


Fig. 10. Comparison of the simulated waveforms of LED output power between multiplier with ideal  $R_S$  and compensated  $R_S$  at (a) different process corners and 27 °C and (b) different temperatures and the typical corner.

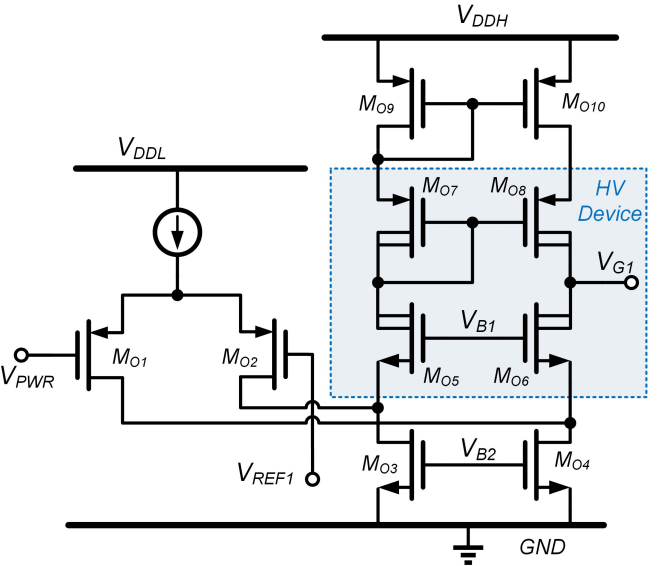


Fig. 11. Circuit diagram of the operational transconductance amplifier.

supplies is developed to meet the requirement of a high gain and high output driving voltage at the same time.  $V_{DDH}$  and  $V_{DDL}$  are designed to 12 and 5 V, respectively. For the input pairs and current mirrors, low voltage devices are employed for good matching, while the cascode transistors are designed with high voltage devices for driving the later high-voltage power transistors with threshold voltage of 2.65 V. In order to open or close these power transistors sequentially, the reference voltages  $V_{REF1}$  to  $V_{REF10}$  for OTAs are designed with slightly increased value. Though a small step for adjacent reference voltage is preferred for small flicker, the step is set

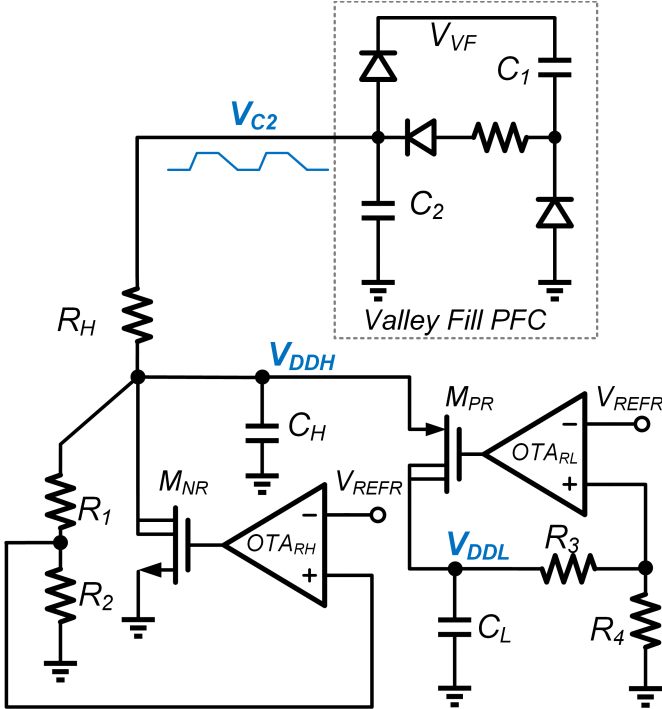


Fig. 12. Circuit diagram of the voltage regulators.

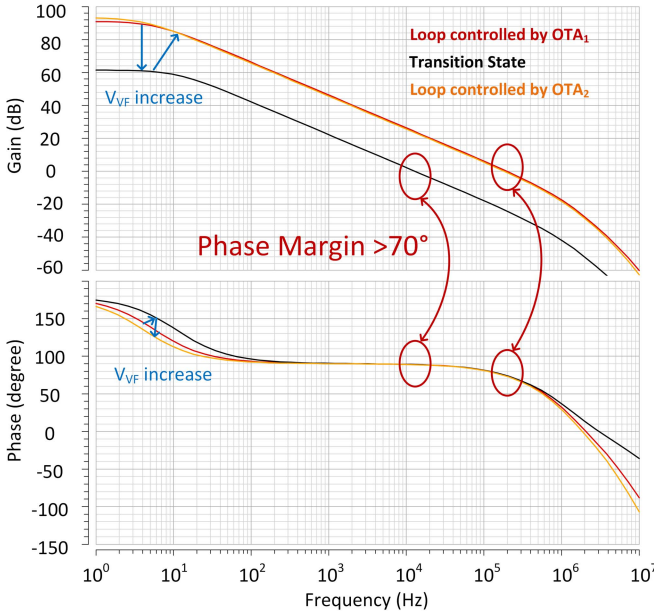


Fig. 13. Simulated loop response at different states for transition from two adjacent branches.

to 20 mV in this design to ensure that the input offset of the OTAs will not affect the switching sequence of the high-voltage power transistors. With the help of off-chip reference voltages  $V_{REF1}$  and  $V_{REF10}$  and on-chip resistor dividers, it is easy to generate other reference voltages from  $V_{REF2}$  to  $V_{REF9}$  for the driver IC.

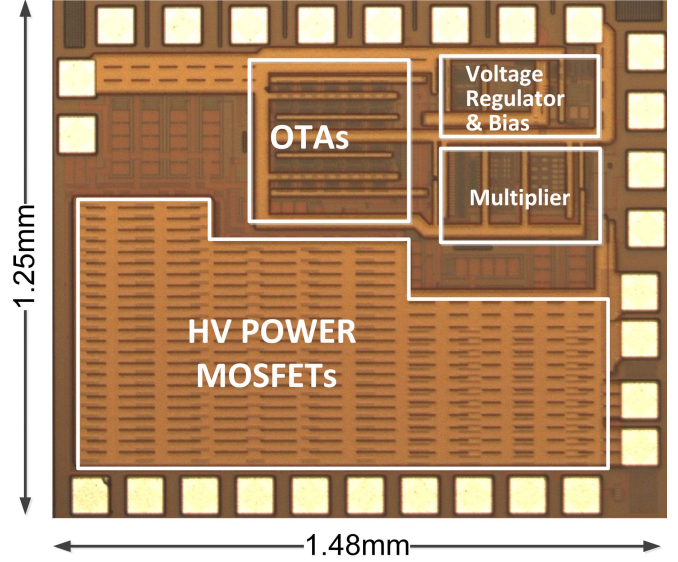


Fig. 14. Chip micrograph of the proposed switching-converter-free driver.

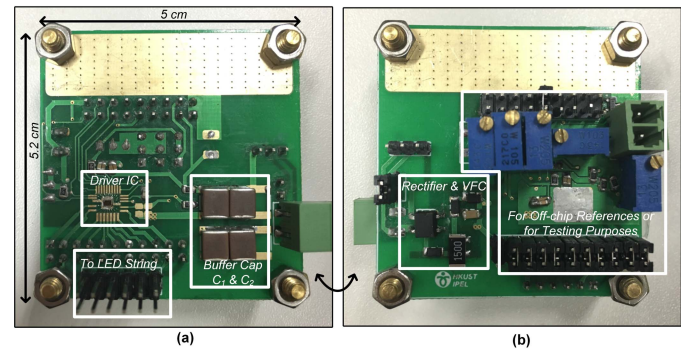


Fig. 15. Test PCB of the proposed driver. (a) Front side. (b) Back side.

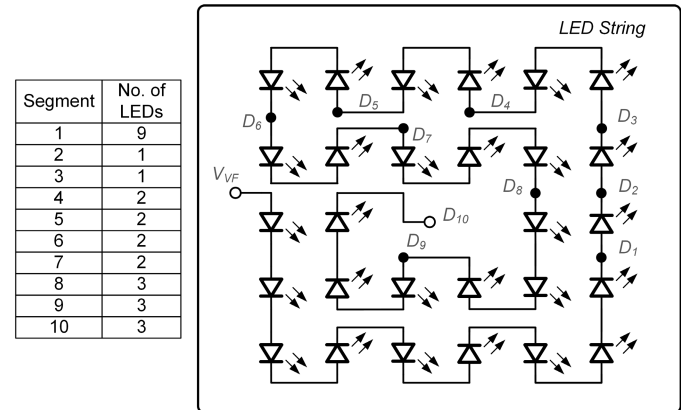


Fig. 16. Layout diagram of LED string on PCB.

#### D. On-Chip Power Supplies

The proposed driver also integrates on-chip regulators to provide power supplies for the whole controller. As shown in Fig. 12, the driver uses  $C_2$  in the valley-fill circuit as the power source instead of directly powering the chip from the high-voltage  $V_{VF}$ . Thus, the step-down ratio of the regulator

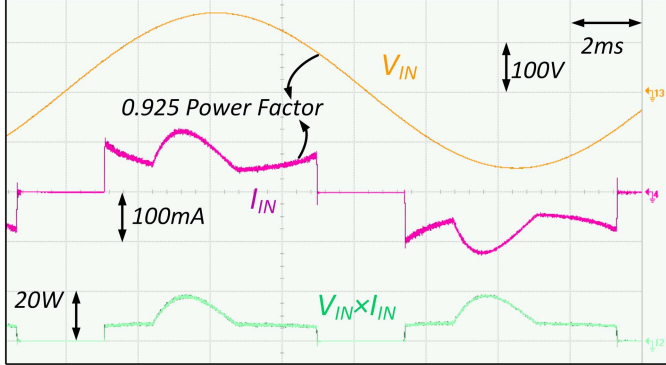


Fig. 17. Measurement results of input current and input voltage at 60-Hz 110-V<sub>ac</sub> 6-W output power.

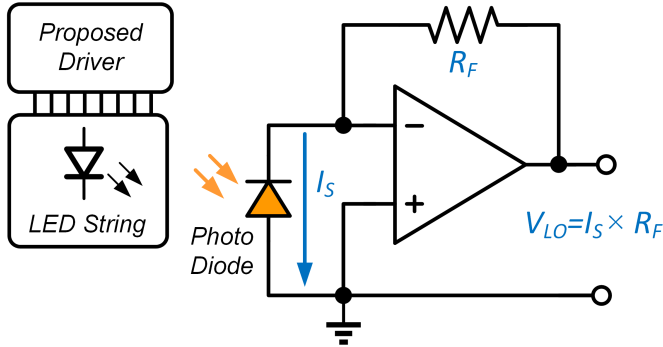


Fig. 18. Optical flicker test circuit.

is reduced, thereby the power loss of the controller. A shunt regulator, formed by  $R_1$ ,  $R_2$ , OTARH, and  $M_{NR}$ , is employed to provide a stable  $V_{DDH}$  (12-V) supply for powering those high-voltage transistors  $M_1$  to  $M_{10}$  in Fig. 5. It is noted that 12 V is chosen, because it is high enough to fully turn ON these transistors, even though they can stand up to 20-V gate voltage. The shunt regulator is followed by a linear regulator, composed of  $R_3$ ,  $R_4$ , OTARL, and  $M_{PR}$ , to offer the low-voltage supply  $V_{DDL}$  (5 V).  $V_{DDL}$  is used for powering all the 5-V on-chip low voltage devices.  $C_H$  and  $C_L$  are two 1- $\mu$ F off-chip capacitors used to ensure the system stability of regulators. The reference voltage  $V_{REFR}$  here is also provided from off-chip in this paper. The total current consumed by the multiplier, OTAs, and bias circuit is around 520  $\mu$ A based on simulation results. As the minimum voltage of  $V_{C2}$  is around 50 V,  $R_H$  is designed to 56 k $\Omega$ . Therefore, besides the power loss of the high-voltage MOSFETS  $M_1$  to  $M_{10}$ , total power consumption of the controller is around 71 mW and most of the power is lost on  $R_H$ . The loss is relatively small compared with the input power for the several watts lighting applications. For comparison, if  $R_H$  is connected to the high voltage node  $V_{VF}$  instead of  $V_{C2}$ , the simulation results show that around 206 mW power will be lost.

#### E. Stability Considerations

The two-branch configuration shown in Fig. 7 is also taken as an example to analyze the system loop stability. For the cases in Fig. 7(a) and (c), the loop is controlled by a single OTA. As  $V_{VF}$  changes in a very low speed (120 Hz),

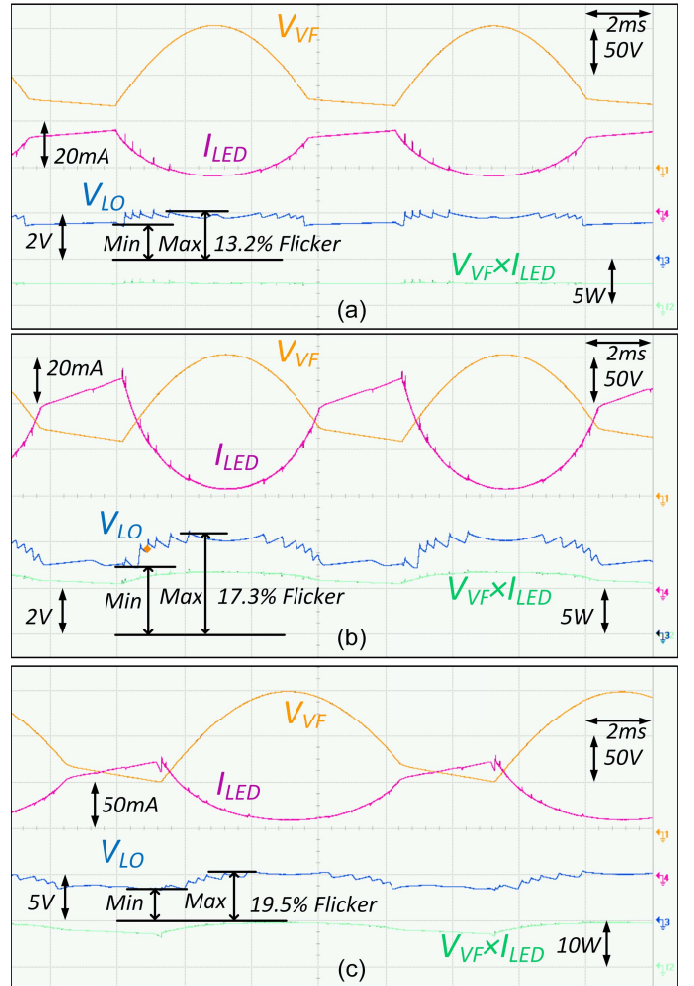


Fig. 19. Measurement results of LED voltage, LED current, and received output light at 60 Hz 110 V<sub>ac</sub>. (a) At 2-W output power. (b) At 6-W output power. (c) At 7.8-W output power.

high loop bandwidth is not required. Therefore, it is flexible to put the dominate pole at the gate of power transistor and utilize a simple dominant pole compensation. The OTAs are designed with low power (below 10  $\mu$ A for each) to reduce the unity-gain-frequency, while most of the power is allocated to the analog multiplier to push the poles in the multiplier to the high frequency. An extra 1.5-pF on-chip capacitor is also added to the output of each OTA to ensure the loop stability. For the situation in Fig. 7(b), two OTAs are competing to control the loop, and in this transition case, some transistors in OTAs are working close to the linear region, resulting in the drop for both gain and unity-gain-frequency. Fig. 13 shows the simulated results of the loop response at different states. Phase margin is kept above 70° during the transition.

## V. MEASUREMENT RESULTS

The proposed driver IC was fabricated with a 0.35- $\mu$ m 120-V high-voltage CMOS process, and the die photograph is shown in Fig. 14. The chip occupies a die area of 1.85 mm<sup>2</sup>, which includes the high-voltage MOSFETs, OTAs, analog multiplier, and on-chip regulators. Besides the driver IC, the system also includes an external diode bridge, a VFC, and

TABLE I  
PERFORMANCE COMPARISON WITH PREVIOUS WORK

	[7]	[10]	[11]	[6]	[18]	[9]	<b>This Work</b>
<b>Year</b>	2013	2013	2012	2015	2012	2011	<b>2016</b>
<b>Process</b>	0.35- $\mu$ m CMOS	1- $\mu$ m 450V BCDMOS	0.5- $\mu$ m 500V LDMOS	Discrete Components	0.35- $\mu$ m BCDMOS	0.5- $\mu$ m 500V BCDMOS	<b>0.35-<math>\mu</math>m 120V HVCMOS</b>
<b>Chip Area</b>	22.1 mm <sup>2</sup>	9.6 mm <sup>2</sup>	3.38 mm <sup>2</sup>	N/A	0.75 mm <sup>2</sup>	3.1 mm <sup>2</sup>	<b>1.85 mm<sup>2</sup></b>
<b>Off-chip Power Switch</b>	HV (>500V) GaN-FET & LV MOSFET	No	No	200V GaN-FET x10	800V MOSFET	No	<b>No</b>
<b>Magnetics</b>	Inductors 850 nH & 12 $\mu$ H	No	No	Inductors 800 nH $\times$ 2	Transformer 1.8 mH	Inductor 5.5 mH	<b>No</b>
<b>HV Capacitor</b>	MLCC 15 $\mu$ F	No	No	MLCC 15 $\mu$ F $\times$ 14 20 $\mu$ F $\times$ 2	Electrolytic 470 $\mu$ F	MLCC 1 $\mu$ F	<b>MLCC 15 <math>\mu</math>F <math>\times</math>4</b>
<b>Power</b>	7-22 W	22 W	9/16 W	30 W	6-12 W	2.5-7 W	<b>2-7.8 W</b>
<b>Input Voltage</b>	110 V <sub>AC</sub>	110/220 V <sub>AC</sub>	110/220 V <sub>AC</sub>	120 V <sub>AC</sub>	180-260 V <sub>AC</sub>	50-320 V <sub>AC</sub>	<b>110 V<sub>AC</sub></b>
<b>Power Factor</b>	0.96	0.99	0.98/0.96	0.9	0.96	0.98/0.92	<b>0.925</b>
<b>Percent Flicker</b>	~100%*	~100%*	~100%*	Not provided	~30%*	~100%*	<b>17.3%<sup>+</sup></b>
<b>Peak Efficiency</b>	89.4%	93.4%	87%	92%	85%	89%	<b>87.6%</b>

\*Estimated from measured current waveform. +Measured with photodiode at 6W output power.

a string of LEDs. In the VFC circuit, the buffer capacitors  $C_1$  and  $C_2$  are designed with the same value and each of them is implemented with two parallel 15- $\mu$ F (nominal) 100-V MLCC capacitors. Fig. 15 shows the test PCB of the proposed driver with a size of 5.2 cm  $\times$  5 cm. It is noted that the core area is less than one fifth of this size, because lots of components and PCB area are used in this demonstration board for providing off-chip voltage references or for testing purposes. These components can be easily removed or integrated into the driver IC. Based on the discussion of the segment optimization in Section IV and (4) and (5), the LED string is implemented with 28 6-V LEDs [16] in series and the string is divided into ten segments, which can be bypassed by the high-voltage transistors. The numbers of LEDs for each segment are 9, 1, 1, 2, 2, 2, 2, 3, 3, and 3, respectively. As the power or output light of each LED from the first to the last segment is gradually reduced, these LEDs are configured into a spiral structure on the PCB, as shown in Fig. 16, to balance the light output in the different directions. The driver can work with an up to 174-V input voltage (123 V<sub>ac</sub>) as there is a voltage drop on the first segment of LEDs (around 54 V). The concept of the QCP control scheme also applies to higher voltage applications, e.g., 220 V<sub>ac</sub>, by choosing a suitable high-voltage process.

Fig. 17 shows the measured waveforms of the ac input voltage and input current at 110 V<sub>ac</sub> and 6-W LED output power. Besides these, the real-time input power is also derived with the help of the waveform calculator in the oscilloscope.

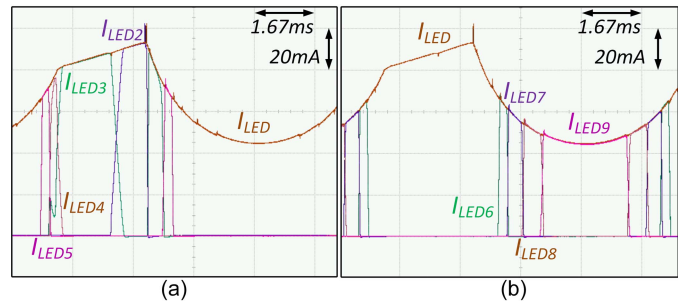


Fig. 20. Measurement results LED current from different power transistors at 60-Hz 110-V<sub>ac</sub> 6-W output power from (a)  $I_{LED2}$  to  $I_{LED5}$  and (b)  $I_{LED6}$  to  $I_{LED9}$ .

A power analyzer is used for the measurement of PF, and 0.925 PF is verified under these testing conditions.

Fig. 18 shows the optical flicker testing circuit. A silicon p-i-n photodiode with good linearity between the reverse current  $I_S$  and the luminance is employed for detecting the light output [17]. The amplifier and feedback resistor  $R_F$  help to transfer the current to voltage  $V_{LO}$ . During the testing, this circuit is placed 0.5 m away from the LED string. Fig. 19 shows the key measured waveforms for the QCP control scheme at different LED powers. The voltage across the LED string  $V_{VF}$ , the LED current  $I_{LED}$ , and their product are shown in each subfigure. Additionally, obtained from the measured waveforms of  $V_{LO}$ , the percent flickers at 2, 6, and 7.8 W

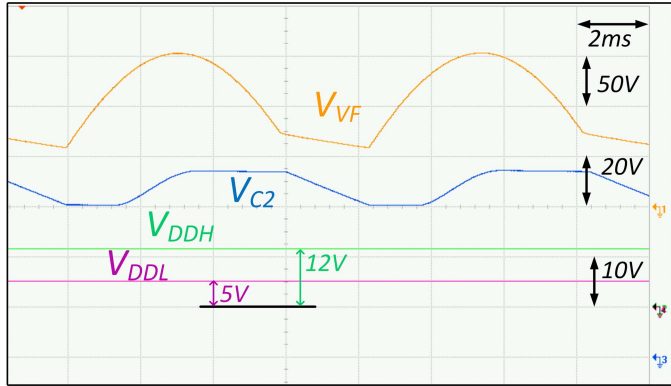


Fig. 21. Measurement results of on-chip regulators.

output are 13.2%, 17.3%, and 19.5%, respectively. Compared with the conventional converter-free LED driver with 100% flicker, an over 80% reduction of flicker is achieved with the proposed design.

The variation of the output light power is due to the following reasons. First, the manually added offset from the voltage references  $V_{REF1}$  to  $V_{REF10}$  contributes 2%–4% of the flicker depending on the reference voltage. Second, as shown in Fig. 6, the effective LED voltage does not exactly follow the voltage  $V_{VF}$ , but goes up and down because some of the power is consumed by the power transistors. This leads to around 6%–7% of the flicker. Third, the LED's light power usually does not increase monotonically with its electrical power, just as shown in Fig. 1. The efficacy will drop at higher LED power. In the case of this paper, this leads to 3%–5% flicker. Finally, both the nonlinearity of the MOSFET-based  $R_S$  and the nonlinearity of the multiplier increase with  $I_{LED}$ , so the percent flicker rises from 13.2% to 19.5% when the LED power goes up from 2 to 7.8 W.

Fig. 20 shows the measured total LED current  $I_{LED}$  and LED current through different power transistors,  $I_{LEDx}$ , in each half cycle. The LED current flows through different power transistors intelligently and sequentially depending on the change of  $V_{VF}$ . It is noted that for the case shown in Fig. 20 under 110 V<sub>ac</sub>, there is no current flowing through power transistor  $M_1$  ( $I_{LED1}$ ) or  $M_{10}$  ( $I_{LED10}$ ) as  $V_{VF}$  does not reach the minimum and maximum voltage designed for the LED string. However, if consider voltage variation from 100 V<sub>ac</sub> to 120 V<sub>ac</sub>, both  $M_1$  and  $M_{10}$  will be activated at different cases. Fig. 21 shows the waveforms of  $V_{VF}$ ,  $V_{C2}$  on the VFC circuit, and power supply  $V_{DDH}$  and  $V_{DDL}$ . These waveforms demonstrate that both the on-chip shunt regulator and linear regulator function normally and the supply voltages are well-regulated regardless of the voltage variation of  $V_{C2}$ .

Fig. 22 shows the plots of the PF, percent flicker, and efficiency at different input voltages and output powers. In most cases, the driver can achieve over 0.9 PF, which meets the requirements of the low to middle power solid-state lighting systems. In addition, the proposed design shows significant improvement in flicker performance compared with the conventional single-stage switching-converter-based drivers and converter-free drivers. The reason for the degradation of the percent flicker at 7.8-W output power and 100 V<sub>ac</sub> is that the

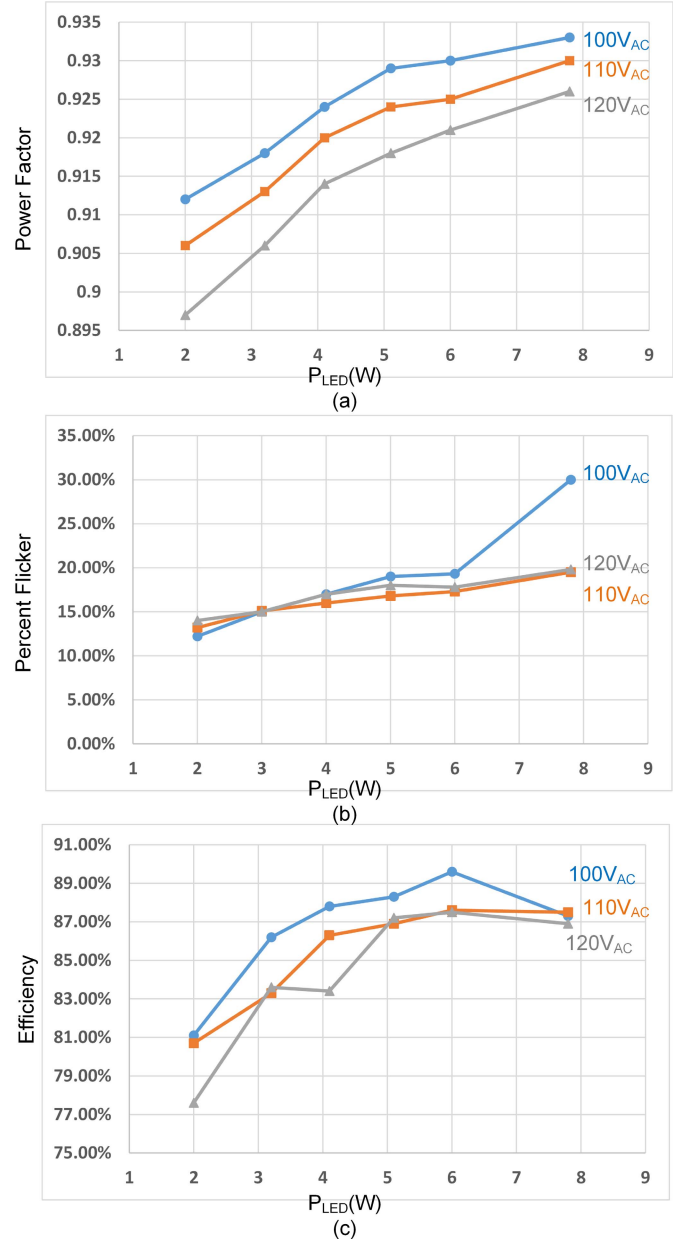


Fig. 22. Measurement results of (a) PF, (b) percent flicker, and (c) efficiency at different input voltages and output powers.

buffer capacitors cannot provide enough voltage for powering the first segment of LEDs in this case. This can be solved with bigger buffer capacitors, or with a reduced number of LED on the first segment, which means higher voltage requirement for the power transistors.

Table I gives a performance comparison of this paper with prior art LED drivers. Most of the existing drivers have to include several bulky off-chip components, such as power transistors, inductors or transformers, and electrolytic capacitors. The proposed design achieves 7.8-W output power regulation capability with only four of 15- $\mu$ F MLCC capacitors, so the total volume for the driver can be greatly reduced. Besides, the proposed driver significantly improves the flicker performance without greatly degrading the PF or efficiency.

## VI. CONCLUSION

An up to 7.8-W output power ac input switching-converter-free LED driver without off-chip transistors, inductors, or electrolytic capacitors is demonstrated in a high-voltage 0.35- $\mu\text{m}$  CMOS technology. The proposed driving solution has the advantages of system miniaturization and rugged reliability. Moreover, with the help of a QCP control scheme, the driver can effectively reduce harmful optical flicker at the double-line-frequency. The percent flicker is reduced by more than 80% compared with conventional switching-converter-free drivers while keeping high efficiency and a good PF. The designed driver achieves 87.6% peak efficiency and an over 0.92 PF with flicker below 20% from a 110-V<sub>ac</sub> 60-Hz input at 2–7.8-W output power range.

## REFERENCES

- [1] ENERGY STAR. *ENERGY STAR Program Requirements for Luminaires—Partner Commitments*, accessed on Apr. 7, 2016. [Online]. Available: [https://www.energystar.gov/ia/partners/product-specs/program\\_reqs/Final\\_Luminaires\\_Program\\_Requirements.pdf](https://www.energystar.gov/ia/partners/product-specs/program_reqs/Final_Luminaires_Program_Requirements.pdf)
- [2] B. Lehman, A. Wilkins, S. Berman, M. Poplawski, and N. J. Miller, “Proposing measures of flicker in the low frequencies for lighting applications,” in *Proc. IEEE Energy Convers. Congr. Expo.*, Sep. 2011, pp. 2865–2872.
- [3] B. Wang, X. Ruan, K. Yao, and M. Xu, “A method of reducing the peak-to-average ratio of LED current for electrolytic capacitor-less AC-DC drivers,” *IEEE Trans. Power Electron.*, vol. 25, no. 3, pp. 592–601, Mar. 2010.
- [4] L. Li *et al.*, “Monolithically integrated drivers for eco-friendly LED system-on-a-chip applications,” in *Proc. IEEE Int. Conf. Electron Devices Solid-State Circuits*, Jun. 2014, pp. 1–2.
- [5] S. Wang, X. Ruan, K. Yao, S.-C. Tan, Y. Yang, and Z. Ye, “A flicker-free electrolytic capacitor-less AC-DC LED driver,” *IEEE Trans. Power Electron.*, vol. 27, no. 11, pp. 4540–4548, Nov. 2012.
- [6] S. Lim, D. M. Otten, and D. J. Perreault, “New AC-DC power factor correction architecture suitable for high-frequency operation,” *IEEE Trans. Power Electron.*, vol. 31, no. 4, pp. 2937–2949, Apr. 2015.
- [7] S. Bandyopadhyay, B. Neidorff, D. Freeman, and A. P. Chandrakasan, “90.6% efficient 11MHz 22W LED driver using GaN FETs and burst-mode controller with 0.96 power factor,” in *IEEE Int. Solid-State Circuits Conf. (ISSCC) Dig. Tech. Papers*, Feb. 2013, pp. 368–369.
- [8] L. Li, Y. Gao, P. K. T. Mok, I.-S. M. Sun, and N. Park, “A 16–28-W 92.8%-efficiency monolithic quasi-resonant LED driver with constant-duty-ratio frequency regulator,” *IEEE Trans. Circuits Syst. II, Express Briefs*, vol. 62, no. 12, pp. 1199–1203, Dec. 2015.
- [9] J. T. Hwang, K. Cho, D. Kim, M. Jung, G. Cho, and S. Yang, “A simple LED lamp driver IC with intelligent power-factor correction,” in *IEEE Int. Solid-State Circuits Conf. (ISSCC) Dig. Tech. Papers*, Feb. 2011, pp. 236–238.
- [10] J. Kim, J. Lee, and S. Park, “A soft self-commutating method using minimum control circuitry for multiple-string LED drivers,” in *IEEE Int. Solid-State Circuits Conf. (ISSCC) Dig. Tech. Papers*, Feb. 2013, pp. 376–377.
- [11] Y.-P. Su *et al.*, “Inductorless and electrolytic capacitorless pseudosine current controller in LED lighting system with 1.1W/2.2W power reduction,” in *Eur. Solid-State Circuits Conf. (ESSCIRC) Dig. Tech. Papers*, Sep. 2012, pp. 442–445.
- [12] J. Kim and S. Park, “Synchronized floating current mirror for maximum LED utilization in multiple-string linear LED drivers,” in *IEEE Int. Solid-State Circuits Conf. (ISSCC) Dig. Tech. Papers*, Jan./Feb. 2016, pp. 232–233.
- [13] Y. Gao, L. Li, and P. K. T. Mok, “A 5.5W AC input converter-free LED driver with 82% low-frequency-flicker reduction, 88.2% efficiency and 0.92 power factor,” in *Proc. Symp. VLSI Circuits*, Jun. 2015, pp. C286–C287.
- [14] G. Han and E. Sanchez-Sinencio, “CMOS transconductance multipliers: A tutorial,” *IEEE Trans. Circuits Syst. II, Analog Digit. Signal Process.*, vol. 45, no. 12, pp. 1550–1563, Dec. 1998.
- [15] Z. Wang, “A CMOS four-quadrant analog multiplier with single-ended voltage output and improved temperature performance,” *IEEE J. Solid-State Circuits*, vol. 26, no. 9, pp. 1293–1301, Sep. 1991.
- [16] *DS207 LUXEON 3030 2D Product Datasheet*, accessed on Apr. 7, 2016. [Online]. Available: <http://www.lumileds.com/uploads/458/DS207-pdf>
- [17] *Silicon PIN Photodiode—BPW34*, accessed on Mar. 22, 2016. [Online]. Available: [http://www.osram-os.com/Graphics/XPic6/00101635\\_0.pdf](http://www.osram-os.com/Graphics/XPic6/00101635_0.pdf)
- [18] J. T. Hwang, M. S. Jung, D. H. Kim, J. H. Lee, M. H. Jung, and J. H. Shin, “Off-the-line primary side regulation LED lamp driver with single-stage PFC and TRIAC dimming using LED forward voltage and duty variation tracking control,” *IEEE J. Solid-State Circuits*, vol. 47, no. 12, pp. 3081–3094, Dec. 2012.



Award in 2017.

**Yuan Gao** (S’13) received the B.Eng. and M.Eng. degrees from Xi’an Jiaotong University, Xi’an, China, in 2009 and 2012, respectively. He is currently pursuing the Ph.D. degree with The Hong Kong University of Science and Technology, Hong Kong.

His current research interests include integrated circuits design for power management and LED lighting system.

Mr. Gao was a recipient of the International Solid-State Circuits Conference Student Travel Grant



**Lisong Li** (S’13) received the B.Sc. degree in electronics engineering and computer science from Peking University, Beijing, China, in 2012. He is currently pursuing the Ph.D. degree with The Hong Kong University of Science and Technology, Hong Kong.

His current research interests include power management integrated circuit design and high-voltage LED driver design.



**Philip K. T. Mok** (S’86–M’95–SM’02–F’14) received the B.A.Sc., M.A.Sc., and Ph.D. degrees from the University of Toronto, Toronto, ON, Canada, in 1986, 1989, and 1995, respectively, all in electrical and computer engineering.

In 1995, he joined the Department of Electronic and Computer Engineering, The Hong Kong University of Science and Technology, Hong Kong, where he is currently a Professor. His current research interests include semiconductor devices, processing technologies, and circuit designs for power electronics and telecommunications applications, with a focus on power management integrated circuits, low-voltage analog integrated circuits, and RF integrated circuits design.

Dr. Mok was a member of the International Technical Program Committees of the IEEE International Solid-State Circuits Conference, from 2005 to 2010 and from 2015 to 2016. He received the Henry G. Acres Medal and the W.S. Wilson Medal from the University of Toronto, and the Teaching Excellence Appreciation Award three times from The Hong Kong University of Science and Technology. He was a co-recipient of the Best Student Paper Award twice in 2002 and 2009 IEEE Custom Integrated Circuits Conference. He served as a Distinguished Lecturer of the IEEE Solid-State Circuits Society from 2009 to 2010, and an Associate Editor of the IEEE JOURNAL OF SOLID-STATE CIRCUITS from 2006 to 2011, the IEEE TRANSACTIONS ON CIRCUITS AND SYSTEMS I from 2007 to 2009 and has served again since 2016, and the IEEE TRANSACTIONS ON CIRCUITS AND SYSTEMS II from 2005 to 2007 and from 2012 to 2015.